metals

Article

Experimental Investigation of Isothermal Section in the La–Co–Ni System at 723 K

Kailin Huang, Liming Xiao, Qingkai Yang, Lu Yang, Zhuobin Li, Zhao Lu *, Qingrong Yao *, Jianqiu Deng, Lichun Cheng, Caimin Huang, Qianxin Long, Jiang Wang and Huaiying Zhou

Guangxi Key Laboratory of Information Materials, School of Material Science and Engineering, Guilin University of Electronic Technology, Guilin 530004, China
* Correspondence: luzhao_gx@163.com (Z.L.); qingry96@guet.edu.cn (Q.Y.)

Abstract: The isothermal section of the La–Co–Ni ternary system at 723 K has been constructed in this work by using X-ray diffraction (XRD), scanning electron microscopy, and energy dispersion spectroscopy techniques (SEM-EDS). The experimental results show no existence of ternary compounds at 723 K. The isothermal section consists of 16 two-phase regions and 8 three-phase regions. La_3Co and La_3Ni, La_2Co_3 and La_2Ni_3, La_2Co_7 and La_2Ni_7, and $LaCo_5$ and $LaNi_5$ form a continuous solid solution. The ternary solid solubility of Ni in $LaCo_{13}$ phase and $La_2Co_{1.7}$ phase was determined to be 15.61 at.% and 9.61 at.%, respectively. The solid solubility of Co in the $LaNi_3$, La_7Ni_3, and LaNi phases was 18.07 at.%, 5.62 at.%, and 8.49 at.%, respectively. The present experimental results are important for the design of La(Fe,Si)$_{13}$-based magnetic refrigeration materials.

Keywords: La–Co–Ni; phase diagram; X-ray diffraction; SEM observation

Citation: Huang, K.; Xiao, L.; Yang, Q.; Yang, L.; Li, Z.; Lu, Z.; Yao, Q.; Deng, J.; Cheng, L.; Huang, C.; et al. Experimental Investigation of Isothermal Section in the La–Co–Ni System at 723 K. *Metals* **2022**, *12*, 1747. https://doi.org/10.3390/met12101747

Academic Editor: Carlos Capdevila-Montes

Received: 12 September 2022
Accepted: 13 October 2022
Published: 17 October 2022

1. Introduction

Magnetic cooling is a novel, energy-efficient, and environmentally friendly technology that aims to replace conventional vapor-compression technology for air conditioning, space heating, and domestic refrigerators/freezers. It is based on the magnetocaloric effect (MCE), which occurs in magnetic materials, in particular those undergoing a magnetic or magneto-structural phase transition [1–3]. The $NaZn_{13}$-type La(Fe,Si)$_{13}$-based alloy system has attracted great attention among reported magnetic refrigerants, as it exhibits tunable giant entropy change and small hysteresis at ambient conditions and contains a minimal amount of rare-earth elements with high Fe-content and high magnetic moment [4,5]. However, its phase transition temperature is around 200 K, so it is difficult to cool it at room temperature. The introduction of transition element Ni can effectively improve the stability of La(FeSi)$_{13}$ compounds, and Co can increase its magnetic phase transition temperature [6–10]. By optimizing the Fe/Co/Ni/Si ratio of the La(FeCoNiSi)$_{13}$ alloy, the magnetic phase transition temperature of the alloy can be adjusted to room temperature, which makes the application of magnetic refrigeration technology at room temperature very possible. Phase diagrams are very important for studying the effects of the elements and are beneficial for alloys in design and fabrication [11–15]. Up to now, however, the current report on the isothermal section of the La–Co–Ni ternary system is the La < 32.2% isothermal section of the La–Co–Ni ternary phase diagram determined by Zheng et al. [16] in 1981, and the phase diagram of La–Co–Ni is not complete. Therefore, here we experimentally determined the isothermal cross-section of the La–Co–Ni ternary system at 723 K.

2. Literature Review

2.1. The La–Co System

The phase diagram of the Co–La system was first studied in detail by Velge [17], who measured the phase diagram of the entire compositional region by metallography, X-ray diffraction, and thermal analysis. The phase formation of La_3Co, $La_2Co_{1.7}$, La_2Co_3, La_2Co_7, $LaCo_5$, and $LaCo_{13}$ was determined at 727 K, 843 K, 968 K, 1073 K, 1363 K, and 1458 K, respectively. After that, the phase diagram was re-investigated by Ray [18], and it was confirmed that $La_2Co_{1.7}$, La_2Co_3, La_2Co_7, $LaCo_5$, and $LaCo_{13}$ were formed by peritectic reaction and found one compound of the La5Co19, which [17] did not report, and the peritectic reaction of La_5Co_{19} was confirmed at a temperature of about 1141 K. In 2006, Wang et al. [19] re-optimized the thermodynamics of the Co–La binary system, and the calculated data were consistent with the experimental results of Buschow and Velge [17]. The calculated phase diagram of the Co–La system is shown in Figure 1a. In 2019, Iwase et al. [20] reported the crystal structure of the compound La_5Co_{19} in detail and found its good hydrogen storage properties.

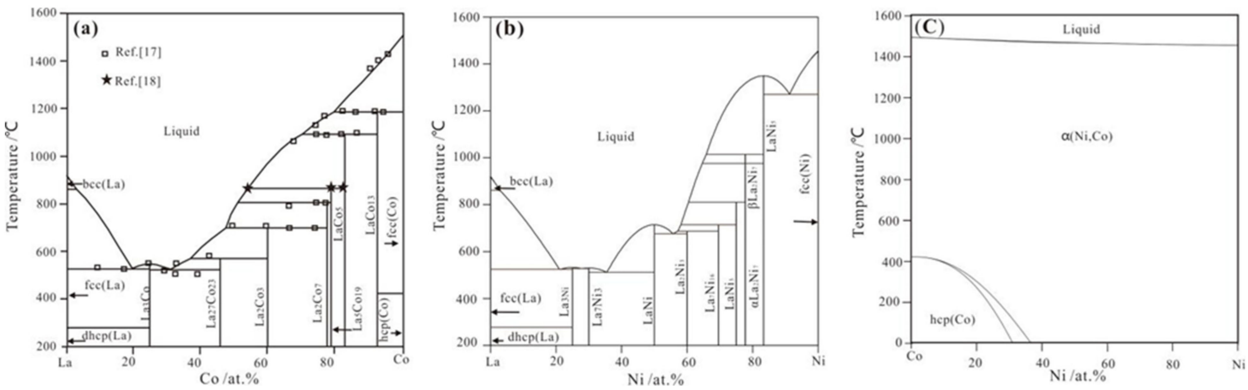

Figure 1. (**a**) The calculated phase diagram of the Co–La system with the experimental data [19]; (**b**) the calculated phase diagram of the La–Ni system [21]; (**c**) the calculated phase diagram of the Co–Ni system [22].

2.2. The La–Ni System

In 1972, Buschow and Mal [23] conducted a detailed study of the Ni–La (50–100 at% Ni) system using thermal analysis, metallography, and X-ray diffraction techniques, and they confirmed the stability of five phases LaNi, $LaNi_{1.4}$, $LaNi_2$, $LaNi_3$, La_2Ni_7, and $LaNi_5$. In 1991, Zhang et al. [24] re-determined the Ni–La binary system phase diagram (50–83.3 at% Ni) and found that the $LaNi_2$ phase could not exist stably, and the $LaNi_{2.286}$ phase was confirmed to be the La_7Ni_{16} phase. In 2003, Zhou et al. [25] studied the phase diagram of the Ni–La–Si ternary system and found that there are eight intermediate compounds at the Ni–La end, namely: La_3Ni, La_7Ni_3, LaNi, La_7Ni_{16}, La_2Ni_3, La_2Ni_7, $LaNi_5$, and $LaNi_3$. In 1998, Du et al. [21] studied the phase diagram of the Ni–La binary system and found nine intermetallic compounds, namely La_3Ni, La_7Ni_3, LaNi, La_7Ni_{16}, La_2Ni_3, La_2Ni_7, βLa_2Ni_7, $LaNi_5$, and $LaNi_3$. The calculated phase diagram of the Co–La system is shown in Figure 1b. In 2000, Dischinger and Schaller [26] used DSC technology to measure the heat capacity of all intermetallic compounds in the La–Ni system at 923~1023 K but did not consider the La_5Ni_{19} phase. In addition, they reported a new phase (La_4Ni_{17}), but this conclusion was not confirmed by other researchers. In 2008, An et al. [27] re-studied the Ni–La binary system and discovered the La_5Ni_{19} phase, which was formed by the peritectic reaction between the liquid phase and the $LaNi_5$ phase at a reaction temperature of 1276 K. In 2017, Subotenko et al. [28] found that $LaNi_2$ is stable at elevated temperatures and decomposes into the La_7Ni_{16} phase below 1003.5 K.

2.3. The Co–Ni System

The Co–Ni system is a simple isomorphous system. It is completely mutually soluble in the whole concentration range of Co and Ni. In 2019, Zhou et al. [22] conducted a thermodynamic evaluation of the Co–Ni–Ta system, where the calculated phase diagram of the Co–Ni system was shown as Figure 1c.

2.4. The La–Co–Ni System

In 1981, a part of the ternary phase diagram of La–Co–Ni (La < 32.2% isothermal section at room temperature) was determined by Zheng [14]. Four single-phase regions were: αCo, βNi, La_3Co, and $LaCo_{5x}Ni_{5-5x}$; five two-phase regions were: αCo + βNi, $LaCo_{13}$ + αCo, $LaCo_{13}$ + βNi, βNi + $LaCo_{5x}Ni_{5-5x}$, $LaCo_{13}$ + $LaCo_{5x}Ni_{5-5x}$; and two three-phase regions were: αCo + βNi + $LaCo_{13}$ and $LaCo_{13}$ + βNi + $LaCo_{5x}Ni_{5-5x}$. Because the phase diagram of the La–Co–Ni system was not verified in detail due to the limitation of the early experimental conditions, this work is based on the study of the phase diagram of the La–Co–Ni system.

The known structures of the single and binary phases are listed in Table 1 [16,17,20,25].

Table 1. The data on the crystal structures of the compounds of the La–Ni, Ni–Co, and La–Co binary systems.

Compound	Pearson Notation	Space Group	Structure Type	Lattice Parameters		Reference
				a (nm)	c (nm)	
$LaCo_{13}$	F112	Fm-3c	$NaZn_{13}$	a = 11.334(1)	—	[17]
$LaCo_5$	hP6	P6/mmm	$CaCu_5$	a = 5.100(5)	c = 3.968(5)	[17]
La_5Co_{19}	hR72	R-3m	Ce_5Co_{19}	a = 5.130(5)	c = 49.50(4)	[20]
La_2Co_7	hR54	R-3m	Gd_2Co_7	a = 5.101(5)	c = 24.511(4)	[17]
La_2Co_3	0S20	Cnca	La_2Ni_3	a = 10.34(1)	c = 7.811(5)	[17]
$La_2Co_{1.7}$	mS8	C2/m	$La_2Co_{1.7}$	a = 8.4536(1)	c = 4.2723(2)	[17]
La_3Co	Op16	pnma	Fe_3C	a = 7.277(9)	c = 6.575(8)	[17]
αCo	Cf4	Fm-3m	Cu	a = 3.5447	—	[16]
βLa	Cf4	Fm-3m	Cu	a = 3.7740	c = 12.171	[16]
La_7Ni_3	—	P63mc	Fe_7Th_3	a = 1.0130	c = 0.6462	[25]
LaNi	—	Cmcm	BCr	a = 0.3907	c = 0.4396	[25]
La_2Ni_3	0S20	Cmca	La_2Ni_3	a = 0.5118	c = 0.7907	[25]
La_7Ni_{16}	—	I42m	La_7Ni_{16}	a = 0.7355	c = 1.451	[25]
$LaNi_3$	—	R3m	$BeNb_3$	a = 0.5086	c = 2.501	[25]
La_2Ni_7	hR55	P63/mmc	Ce_2Ni_7	a = 0.5085	c = 2.471	[25]
$LaNi_5$	—	P6/mmm	$CaCu_5$	a = 0.5016	c = 0.3983	[25]
βNi	Cf4	Fm-3m	Cu	a = 3.5446	—	[25]

3. Experimental Procedure

The phase relationships of the La–Co–Ni ternary system were constructed by equilibrated alloys. High purity of La (99.99%), Co (99.99%), and Ni (99.99%) were used as raw materials. The alloys with the mass of 3 g were prepared by arc melting with a non-consumable tungsten electrode under the protection of a high-purity argon atmosphere. The samples were turned over and re-melted four times to improve alloy homogeneities. The melting loss was less than 1 mass.%. The alloys were annealed at 723 K for 1440 h. After that, the samples were taken from the muffle furnace and quenched quickly in ice water.

The phase consistence and crystal structure of the samples were identified by means of XRD (Rigaku D/max2550VB, Tokyo, Japan) using Cu Kα radiation. The diffractometer was operated at 40 kV and 40 mA, and the 2θ scan ranges from 20° to 90° with a step size of 0.02° and a counting time of 5 s per step. The microstructural features and the elemental distribution of the alloy were characterized using SEM-EDS and XRD methods.

4. Results and Discussion

4.1. Microstructure

The twenty-two La–Co–Ni alloys annealed at 723 K for 1440 h were examined by SEM-EDS and XRD. It should be noted that the accuracy of the EDS results is about 0.01%. The experimental results of phase compositions measured by EDS and phase identified by XRD are presented in Table 2. Figure 2 shows SEM images and XRD patterns of the representative La–Co–Ni alloys annealed at 723 K for 1440 h. According to the SEM-EDS results and the XRD analysis, it can be seen in Figure 2a that alloy #5 ($La_{85}Co_5Ni_{10}$) was composed of La_3(Co,Ni) and βLa phases, which agrees with the results of XRD results. The light-gray phase and white phase in Figure 2a correspond to the βLa and La_3(Co,Ni) phases, respectively. Their compositions were $La_{73.21}Co_{17.30}Ni_{9.49}$ and $La_{94.53}Co_{4.21}Ni_{1.21}$, respectively. So, the alloy $La_{85}Co_5Ni_{10}$ is confirmed to be located in the two-phase region, La_3(Co,Ni) + βLa. The BSE image of the no. 6 ($La_{62}Co_6Ni_{32}$) sample is presented in Figure 2b, showing the co-existence of two-phase $La_7(Co,Ni)_3$ (white) + LaNi(gray). Their compositions are $La_{68.79}Co_{5.62}Ni_{25.59}$ and $La_{49.61}Co_{3.37}Ni_{47.02}$, respectively. The result is consistent with the XRD results. So, the alloy $La_{62}Co_6Ni_{32}$ is confirmed to be located in the two-phase region, La_7Ni_3 + LaNi. The BSE image of the no. 1 ($La_9Co_{85}Ni_6$) sample annealed at 723 K for 1440 h is presented in Figure 2c, showing the co-existence of the three-phase area $LaCo_5$(white) + $LaCo_{13}$(gray) + αCo(black). The result is consistent with the XRD results. Figure 2d presents the BSE image of the no. 4 ($La_{68}Co_{26}Ni_6$) sample alloy annealed at 723 K for 1440 h. The white and gray phases are the La_3(Co,Ni) phase and $La_2Co_{1.7}$ phase. The no. 18 ($La_{34}Co_{11}Ni_{55}$) sample displays the alloy that consists of the La_2Ni_3(white) and $LaNi_3$(gray) phase in Figure 2f. The XRD pattern identified the result, as can be seen in Figure 2e, and their compositions are $La_{40.22}Co_{3.63}Ni_{56.15}$, $La_{25.90}Co_{17.99}Ni_{56.11}$, and $La_{22.96}Co_{29.03}Ni_{48.01}$, respectively. Figure 2g,h shows BSE images and XRD patterns of the no. 12 ($La_8Co_{10}Ni_{82}$) sample annealed at 723 K for 1440 h. According to the SEM-EDS results and the XRD analysis, it can be seen in Figure 2h that alloy #12 ($La_8Co_{10}Ni_{82}$) was composed of $LaNi_5$ and βNi phases, which agrees with the results of XRD results, as can be seen in Figure 2g.

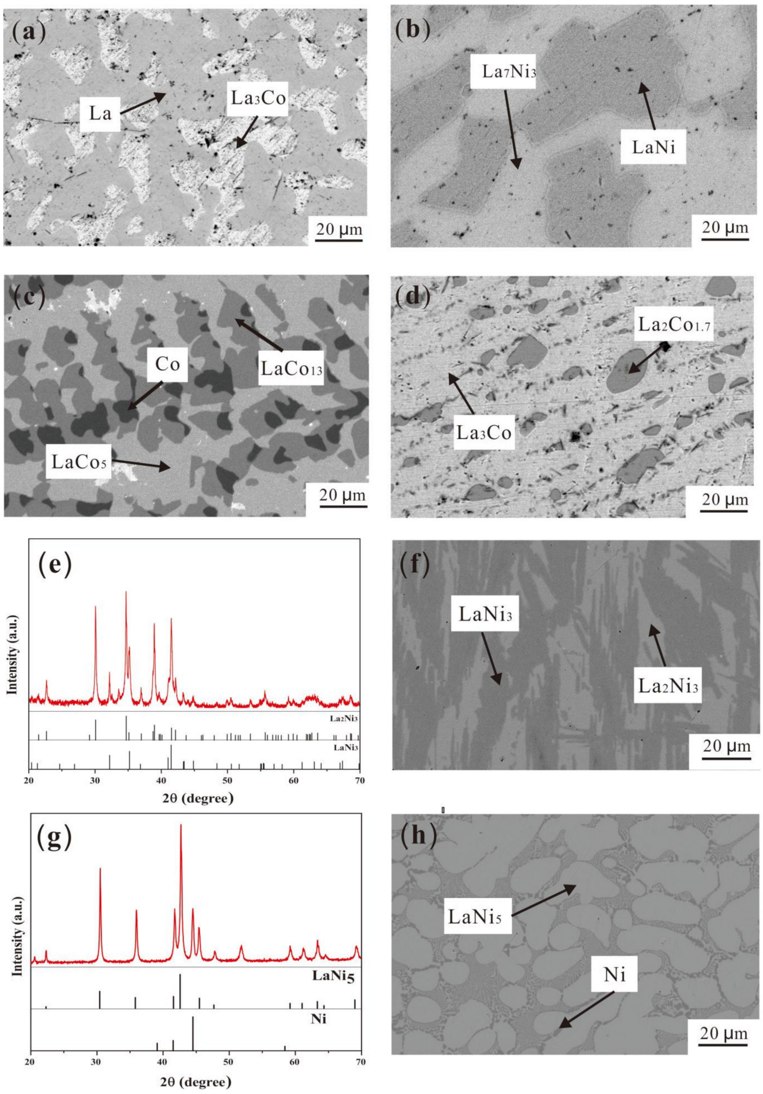

Figure 2. The XRD pattern and SEM micrograph for alloys annealed at 723 K for 60 days: (**a**) no. 5 ($La_{85}Co_5Ni_{10}$); (**b**) no. 6 ($La_{62}Co_6Ni_{32}$); (**c**) no. 1 ($La_9Co_{85}Ni_6$); (**d**) no. 4 ($La_{68}Co_{26}Ni_6$); (**e**,**f**) no. 18 ($La_{34}Co_{11}Ni_{55}$); (**g**,**h**) no. 12 ($La_8Co_{10}Ni_{82}$).

Table 2. Composition of the La–Co–Ni phases according to the EDS data.

Alloy	Nominal Composition (at.%)	EDS Measurement				XRD Results
		La (at.%)	Co (at.%)	Ni (at.%)	Phase	
1	$La_9Co_{85}Ni_6$	16.06	72.30	11.65	$LaCo_5$	$LaCo_5$
		0.01	95.31	4.68	αCo	αCo
		6.92	77.47	15.61	$LaCo_{13}$	$LaCo_{13}$
2	$La_7Co_{44}Ni_{49}$	15.41	72.13	12.46	$LaCo_5$	$LaCo_5$
		0.40	95.03	4.56	αCo	αCo
		0.50	14.20	85.30	βNi	βNi
3	$La_{12}Co_{60}Ni_{28}$	0.01	94.31	5.68	αCo	αCo
		16.06	71.3	12.65	$LaCo_5$	$LaCo_5$
4	$La_{68}Co_{26}Ni_6$	53.79	43.07	3.13	$La_2Co_{1.7}$	$La_2Co_{1.7}$
		72.54	16.76	10.70	La_3Co	La_3Co
5	$La_{85}Co_5Ni_{10}$	73.21	17.30	9.49	La_3Co	La_3Co
		94.53	4.21	1.26	βLa	βLa
6	$La_{62}Co_6Ni_{32}$	68.79	5.62	25.59	La_7Ni_3	La_7Ni_3
		49.61	3.37	47.02	LaNi	LaNi
7	$La_{51}Co_{34}Ni_{15}$	40.53	45.79	13.68	La_2Co_3	La_2Co_3
		49.73	8.49	41.78	LaNi	LaNi
		52.73	37.66	9.61	$La_2Co_{1.7}$	$La_2Co_{1.7}$
8	$La_{44}Co_{12}Ni_{44}$	40.35	17.96	41.69	La_2Ni_3	La_2Ni_3
		50.67	8.49	40.84	LaNi	LaNi
9	$La_{44}Co_{49}Ni_7$	53.15	41.63	5.22	$La_2Co_{1.7}$	$La_2Co_{1.7}$
		41.53	50.08	8.39	La_2Co_3	La_2Co_3
10	$La_{70}Co_5Ni_{25}$	70.41	5.45	24.14	La_7Ni_3	La_7Ni_3
		72.54	10.76	16.70	La_3Ni	La_3Ni
		49.45	1.28	49.26	LaNi	LaNi
11	$La_{72}Co_5Ni_{23}$	70.41	5.06	24.53	La_7Ni_3	La_7Ni_3
		72.86	5.62	21.53	La_3Ni	La_3Ni
12	$La_8Co_{10}Ni_{82}$	17.51	25.20	57.29	$LaNi_5$	$LaNi_5$
		0.05	5.37	94.58	βNi	βNi
13	$La_8Co_{90}Ni_2$	7.41	77.26	15.33	$LaCo_{13}$	$LaCo_{13}$
		0.40	95.03	4.56	αCo	αCo
14	$La_{10}Co_{88}Ni_2$	16.06	70.30	13.66	$LaCo_5$	$LaCo_5$
		7.41	77.26	15.33	$LaCo_{13}$	$LaCo_{13}$
15	$La_{33}Co_{24}Ni_{43}$	40.12	21.01	38.87	$La_2(Co,Ni)_3$	$La_2(Co,Ni)_3$
		22.96	29.03	48.01	$La_2(Co,Ni)_7$	$La_2(Co,Ni)_7$
16	$La_{31}Co_{42}Ni_{27}$	39.80	41.12	19.08	$La_2(Co,Ni)_3$	$La_2(Co,Ni)_3$
		22.83	45.98	31.19	$La_2(Co,Ni)_7$	$La_2(Co,Ni)_7$
17	$La_{30}Co_{63}Ni_7$	39.12	56.13	7.75	$La_2(Co,Ni)_3$	$La_2(Co,Ni)_3$
		22.67	69.83	7.50	$La_2(Co,Ni)_7$	$La_2(Co,Ni)_7$
18	$La_{34}Co_{11}Ni_{55}$	40.20	10.10	49.70	La_2Ni_3	La_2Ni_3
		25.52	18.07	56.41	$LaNi_3$	$LaNi_3$
19	$La_{36}Co_3Ni_{61}$	40.22	3.63	56.15	La_2Ni_3	La_2Ni_3
		30.50	2.82	66.68	La_7Ni_{16}	La_7Ni_{16}
20	$La_{29}Co_4Ni_{67}$	30.49	4.98	64.53	La_7Ni_{16}	La_7Ni_{16}
		25.90	17.99	56.11	$LaNi_3$	$LaNi_3$
21	$La_{60}Co_{19}Ni_{21}$	74.93	6.62	18.45	La_3Ni	La_3Ni
		50.12	6.71	43.17	LaNi	LaNi
		53.94	36.45	9.61	$La_2Co_{1.7}$	$La_2Co_{1.7}$
22	$La_{57}Co_{14}Ni_{29}$	74.98	6.67	18.35	La_3Ni	La_3Ni
		50.67	8.49	40.84	LaNi	LaNi
		53.43	37.67	8.90	$La_2Co_{1.7}$	$La_2Co_{1.7}$

4.2. Isothermal Section for La–Co–Ni at 723 K

Based on the experimental results obtained in this work and the information of relevant binary systems taken from the literature, the isothermal section of the La–Co–Ni system at 723 K in the whole concentration region was constructed and is shown in Figure 3. La_3Co, $La_2Co_{1.7}$, La_2Co_3, La_2Co_7, $LaCo_5$, La_5Co_{19}, $LaCo_{13}$, La_3Ni, La_7Ni_3, LaNi, La_7Ni_{16}, La_2Ni_7, $LaNi_5$, and $LaNi_3$ phases were found to be stable at 723 K. Among them, La_3Co and La_3Ni, La_2Co_3 and La_2Ni_3, La_2Co_7 and La_2Ni_7, and $LaCo_5$ and $LaNi_5$ form continuous solid solutions. The ternary solid solubility of Ni in the $LaCo_{13}$ phase and $La_2Co_{1.7}$ phase is about 15.61 at.% and 9.61 at.%, respectively. In addition, the ternary solid solubility of Co in the $LaNi_3$ phase, La_7Ni_3 phase, and LaNi phase are about 18.07 at.%, 5.62 at.%, and 8.49 at.%, respectively. No ternary compounds were found. Unfortunately, the phase region in the dotted line cannot be determined because the relevant sample is not balanced. The system consists of 16 two-phase regions and 8 three-phase regions. In contrast to the room-temperature isothermal cross-section [28], in the region of La < 32.2%, βNi in the single-phase region of αCo can be solubilized at room temperature, and the cross-section at this temperature is αCo + βNi + $La(Co,Ni)_5$ in the three-phase region. There is the $LaCo_{13}$ + βNi + $LaCo_5$ three-phase region at room temperature, which transforms the $LaCo_{13}$ + αCo + $LaCo_5$ three-phase region at 723 K. In addition, the two-phase region αCo + βNi and the three-phase region αCo + βNi + $LaCo_{13}$ disappeared at 723 K and were replaced by the two-phase region αCo + $La(Co,Ni)_5$. Furthermore, the solid solution limit of βNi in $LaCo_{13}$ is found to be 15.61 at.% by means of the no. 1 sample.

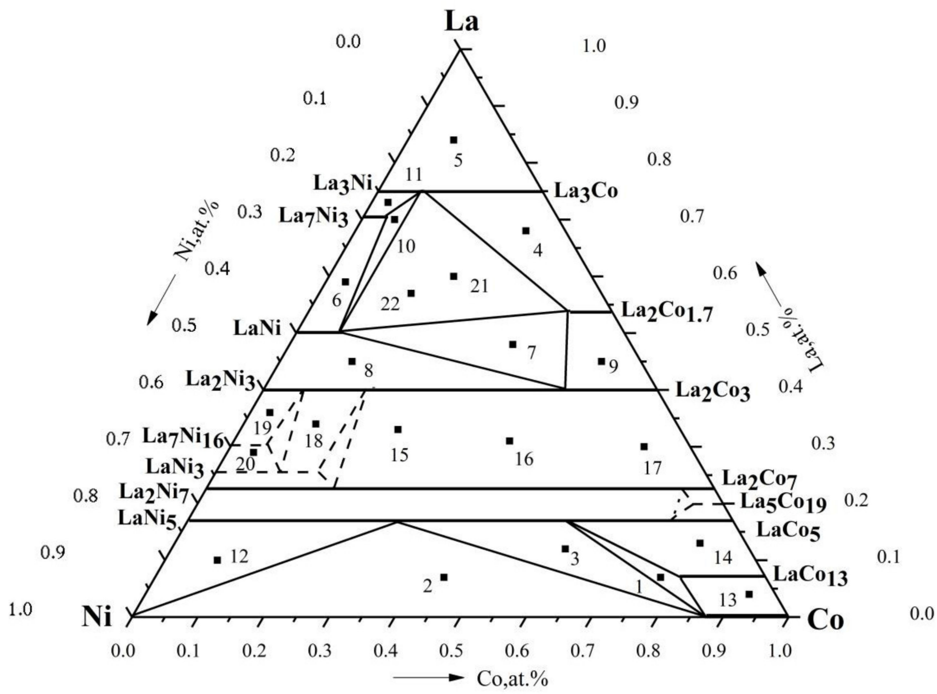

Figure 3. Isothermal section of the La–Co–Ni system at 723 K (in the whole concentration region).

The eight three-phase regions are: La_3Ni + La_7Ni_3 + LaNi, La_7Ni_{16} + La_2Ni_3 + $LaNi_3$, LaNi + La_2Co_3 + $La_2Co_{1.7}$, LaNi + La_3Ni + $La_2Co_{1.7}$, αCo + βNi + $La(Co,Ni)_5$, La_2Ni_3 + $LaNi_3$ + La_2Ni_7, $LaCo_{13}$ + αCo + $LaCo_5$, and La_2Co_7 + La_5Co_{19} + $LaCo_5$. The 16 two-phase regions are: $La_3(Co,Ni)_5$ + βLa, La_3Ni + La_7Ni_3, La_7Ni_3 + LaNi, La_2Co_3 + $La_2Co_{1.7}$, La_3Co + $La_2Co_{1.7}$, LaNi + La_3Ni + $La_2Co_{1.7}$, La_2Ni_3 + LaNi, $LaCo_{13}$ + $LaCo_5$, La_2Co_7 + La_2Co_3, $LaCo_{13}$ + αCo, $LaCo_5$ + αCo, βNi + $LaNi_5$, La_2Ni_3 + La_7Ni_{16}, $LaNi_3$ + La_7Ni_{16}, La_2Ni_3 + La_2Ni_7, and $LaNi_3$ + La_2Ni_3.

5. Conclusions

In this work, phase equilibria in the La–Co–Ni system at 723 K were measured using equilibrated alloy samples. Eight three-phase regions and sixteen two-phase regions were determined in the isothermal sections of the La–Co–Ni ternary system. La_3Co and La_3Ni, La_2Co_3 and La_2Ni_3, La_2Co_7 and La_2Ni_7, and $LaCo_5$ and $LaNi_5$ form a continuous solid solution. The ternary solid solubility of Ni in the $LaCo_{13}$ phase and $La_2Co_{1.7}$ phase is about 15.61 at.% and 9.61 at.%, respectively. In addition, the ternary solid solubility of Co in the $LaNi_3$ phase, La_7Ni_3 phase, and LaNi phase is about 18.07 at.%, 5.62 at.%, and 8.49 at.%, respectively. No ternary compounds were found.

Author Contributions: Data curation, K.H.; formal analysis, K.H., L.X., Q.Y. (Qingkai Yang), L.Y., Z.L. (Zhuobin Li), Z.L. (Zhao Lu) and Q.Y. (Qingrong Yao); investigation, K.H. and L.X.; methodology, K.H., L.X., Q.Y. (Qingkai Yang), L.Y. and Z.L. (Zhuobin Li); software, K.H.; writing—original draft preparation, K.H.; writing—review and editing, Z.L. (Zhao Lu); project administration, Z.L. (Zhao Lu) and Q.Y. (Qingrong Yao); Contribution to the design, Z.L. (Zhao Lu), Q.Y. (Qingrong Yao), J.D., L.C., C.H., Q.L., J.W. and H.Z.; interpretation of data, J.D., L.C., C.H., Q.L., J.W. and H.Z. All authors have read and agreed to the published version of the manuscript.

Funding: This work was supported by the National Natural Science Foundation of China (grant nos.: 52061007 and 52261004), the Science and Technology Project of Guangxi (grant nos.: AB21220028, AA22068084, AA18242023, and AD21220018), the Natural Science Foundation of Guangxi (grant no.: 2021GXNSFDA075009), Guangxi Key Laboratory of Information Materials (grant nos.:191012-Z and 211034-Z), basic scientific research of young teachers in Guangxi universities (grant no.: 2021KY0198), and the innovation program for University students (grant no.: 201910595037) are acknowledged.

Institutional Review Board Statement: Not applicable.

Informed Consent Statement: Not applicable.

Data Availability Statement: Not applicable.

Conflicts of Interest: The authors declare no conflict of interest.

References

1. Gutfleisch, O.; Willard, M.A.; Brück, E.; Chen, C.H.; Sankar, S.G.; Liu, J.P. Magnetic Materials and Devices for the 21st Century: Stronger, Lighter, and More Energy Efficient. *Adv. Mater.* **2010**, *23*, 821–842. [CrossRef] [PubMed]
2. Pecharsky, V.K.; Gschneidner, K.A., Jr. Giant magnetocaloric effect in Gd5(Si2Ge2). *Phys. Rev. Lett.* **1997**, *78*, 4494–4497. [CrossRef]
3. Shen, B.G.; Sun, J.R.; Hu, F.X.; Zhang, H.W.; Cheng, Z.H. Recent Progress in Exploring Magnetocaloric Materials. *Adv. Mater.* **2009**, *21*, 4545–4564. [CrossRef]
4. Tušek, J.; Kitanovski, A.; Tomc, U.; Favero, C.; Poredoš, A. Experimental comparison of multi-layered La–Fe–Co–Si and single-layered Gd active magnetic regenerators for use in a room-temperature magnetic refrigerator. *Int. J. Refrig.* **2014**, *37*, 117–126. [CrossRef]
5. Jacobs, S.; Auringer, J.; Boeder, A.; Chell, J.; Komorowski, L.; Leonard, J.; Russek, S.; Zimm, C. The performance of a large-scale rotary magnetic refrigerator. *Int. J. Refrig.* **2014**, *37*, 84–91. [CrossRef]
6. Ido, H.; Sohn, J.C.; Pourarian, F.; Cheng, S.F.; Wallace, W.E. Magnetic properties of LaCo13-based systems. *J. Appl. Phys.* **1990**, *67*, 4978–4980. [CrossRef]
7. Nikitin, S.; Tereshina, I.; Verbetsky, V.; Salamova, A.; Anosova, E. Synthesis and properties of NaZn13-type interstitial compounds. *J. Alloys Compd.* **2004**, *367*, 266–269. [CrossRef]
8. Hu, F.X.; Gao, J.; Qian, X.L.; Ilyn, M.; Tishin, A.M.; Sun, J.R.; Shen, B.G. Magnetocaloric effect in itinerant electron metamagnetic systems La(Fe1−xCox)11.9Si1.1. *J. Appl. Phys.* **2005**, *97*, 10M303. [CrossRef]
9. Sun, S.; Ye, R.; Long, Y. Influence of the substitution of Ni for Fe on the microstructure evolution and magnetic phase transition in La(Fe1−xNix)11.5Si1.5 compounds. *Mater. Sci. Eng. B* **2013**, *178*, 60–64. [CrossRef]
10. Moreno-Ramírez, L.M.; Romero-Muñiz, C.; Law, J.Y.; Franco, V.; Conde, A.; Radulov, I.A.; Maccari, F.; Skokov, K.P.; Gutfleisch, O. The role of Ni in modifying the order of the phase transition of La(Fe,Ni,Si)13. *Acta Mater.* **2018**, *160*, 137–146. [CrossRef]
11. Fartushna, I.; Mardani, M.; Khvan, A. *Experimental Investigation of Fe–Co–La System: Liquidus and Solidus Projections*; Springer: Berlin/Heidelberg, Germany, 2020.
12. Fartushna, I.; Mardani, M.; Khvan, A.; Cheverikin, V.; Kondratiev, A. Experimental investigation of phase equilibria in the Co–Fe–La system at 600 and 500 °C. *Calphad* **2020**, *70*, 101794. [CrossRef]
13. Huang, S.X.; Zhang, X.D.; Jiang, Y.; Jiang, Y.R.; Mao, C.; Wu, D.; Zhang, L.G.; Liu, L.B. Experimental Investigation of Ti–Nb–Co Ternary System at 1000 °C. *Mater. Des.* **2017**, *115*, 170–178. [CrossRef]
14. Schmid-Fetzer, R. Phase Diagrams: The Beginning of Wisdom. *J. Phase Equilib. Diffus.* **2014**, *35*, 735–760. [CrossRef]
15. Chen, X.; Chen, Y.G.; Tang, Y.B. Effect of Ce, Co, B on formation of LaCo_(13)-structure phase in La(Fe,Si)_(13) alloys. *Trans. Nonferrous Met. Soc. China* **2014**, *24*, 705–711. [CrossRef]
16. Jian-Xuan, Z.; Guo-Yun, L. A Phase Diagram of The La-Co-Ni Ternary System. *Acta Phys. Sin.* **1982**, *31*, 674–679. [CrossRef]
17. Buschow, K.; Velge, W. Phase relations and intermetallic compounds in the lanthanum-cobalt system. *J. Less Common Met.* **1967**, *13*, 11–17. [CrossRef]
18. Ray, A.E. A Review of the Binary Rare Earth-Cobalt Alloy Systems. *Am. Inst. Phys.* **1974**, *18*, 1143. [CrossRef]
19. Wang, C.P.; Wang, J.; Liu, X.J.; Ohnuma, I.; Kainuma, R.; Ishida, K. Thermodynamic assessment of the Co-La and Mo-La systems. *J. Alloys Compd.* **2008**, *453*, 174–179. [CrossRef]
20. Iwase, K.; Ueno, T.; Mori, K. Crystal structure and hydrogen absorption− desorption property of La5Co19. *Int. J. Hydrog. Energy* **2019**, *44*, 23172–23178. [CrossRef]

21. Du, Z.; Wang, D.; Zhang, W. Thermodynamic assessment of the La-Ni system. *J. Alloys Compd.* **1998**, *264*, 209–213. [CrossRef]
22. Zhou, C.; Guo, C.; Li, C.; Du, Z. Thermodynamic description of the Co–Ni–Ta system. *Calphad* **2019**, *66*, 101649. [CrossRef]
23. Buschow, K.H.; Mal, H. Phase relations and hydrogen absorption in the lanthanum-nickel system. *J. Less-Common Met.* **1972**, *29*, 203–210. [CrossRef]
24. Zhang, D.; Tang, J.; Gschneidner, K.A. A redetermination of the La-Ni phase diagram from LaNi to LaNi5 (50-83.3 at.% Ni). *J. Less Common Met.* **1991**, *169*, 45–53.
25. Zhou, H.; Yao, Q.; Yuan, S.; Liu, J.; Deng, H. Phase relationships in the La–Ni–Si system at 673 K. *J. Alloys Compd.* **2004**, *366*, 161–164. [CrossRef]
26. Dischinger, J.; Schaller, H.J. On the constitution and thermodynamics of Ni–La alloys. *J. Alloys Compd.* **2000**, *312*, 201–210. [CrossRef]
27. An, X.H.; Gu, Q.F.; Zhang, J.Y.; Chen, S.L.; Yu, X.B.; Li, Q. Experimental investigation and thermodynamic reassessment of La–Ni and LaNi5–H systems. *Calphad* **2013**, *40*, 48–55. [CrossRef]
28. Subotenko, P.M.; Kudin, V.G.; Shevchenko, M.O.; Ivanov, M.I.; Berezutskii, V.V.; Sudavtsova, V. SThermodynamic properties of La–Ni alloys. *Powder Metall. Met. Ceram.* **2017**, *55*, 717–725. [CrossRef]